Colloids and Surfaces B: Biointerfaces 133 (2015) 66–72

Contents lists available at ScienceDirect

Colloids and Surfaces B: Biointerfaces

journal homepage: www.elsevier.com/locate/colsurfb

Determination of binding capacity and adsorption enthalpy between Human Glutamate Receptor (GluR1) peptide fragments and kynurenic acid by surface plasmon resonance experiments. Part 2: Interaction of $GluR1_{270–300}$ with KYNA

E. Csapó[a,*], F. Bogár[a], Á. Juhász[a], D. Sebők[a], J. Szolomájer[a], G.K. Tóth[b], Z. Majláth[c], L. Vécsei[c,d], I. Dékány[a,b,*]

[a] MTA-SZTE Supramolecular and Nanostructured Materials Research Group, University of Szeged, H-6720 Dóm tér 8, Szeged, Hungary
[b] Department of Medical Chemistry, Faculty of Medicine, University of Szeged, H-6720 Dóm tér 8, Szeged, Hungary
[c] Department of Neurology, University of Szeged, H-6725 Semmelweis u. 6, Szeged, Hungary
[d] MTA-SZTE Neuroscience Research Group, University of Szeged, H-6725 Semmelweis u. 6, Szeged, Hungary

ARTICLE INFO

Article history:
Received 16 February 2015
Received in revised form 14 April 2015
Accepted 20 April 2015
Available online 4 June 2015

Keywords:
Kynurenic acid
Glutamate receptor
Binding enthalpy
Molecular docking
SPR
AFM

ABSTRACT

In the course of our previous work, the interactions of two peptide fragments ($GluR1_{201–230}$ and $GluR1_{231–259}$) of human glutamate receptor ($GluR1_{201–300}$) polypeptide with kynurenic acid (KYNA) were investigated by surface plasmon resonance (SPR) spectroscopy. Besides quantitation of the interactions, the enthalpies of binding of KYNA on certain peptide fragment-modified gold surfaces were also reported. In the present work, a third peptide fragment ($GluR1_{270–300}$) of the glutamate receptor was synthesized and its interaction with KYNA was investigated by an SPR technique. This 31-membered peptide was chemically bonded onto a gold-coated SPR chip *via* a cysteine residue. The peptide-functionalized biosensor chip was analyzed by atomic force microscopy (AFM) and theoretical calculations were performed on the structure and dimensions of the peptide on the gold surface. In order to determine the isosteric heat of adsorption of the binding of KYNA on the peptide-functionalized gold thin film, SPR experiments were carried out between +10 °C and +40 °C. The results on the $GluR1_{270–300}$–KYNA system were compared with the previously published binding parameters of the interactions of $GluR1_{201–230}$ and $GluR1_{231–259}$ with KYNA. The binding abilities of KYNA with all three peptide fragments immobilized on the gold surface were estimated by a molecular docking procedure and the binding free energies of these AMPA receptor subunits with KYNA were determined.

1. Introduction

A number of label-free, *in situ* detection techniques have been developed to monitor antibody–antigen, DNA–DNA, DNA–protein, receptor–ligand, protein–cell, etc. interactions [1,2]. The surface plasmon resonance (SPR) technique has been widely used to monitor biomolecular interactions on a gold surface [3–7]. One of the interactants is immobilized from solution onto a solid/liquid interface, and a solution of the other interactant is passed over the surface. During this procedure, the refractive index at the interface undergoes change, this being directly related to the amount of the biomolecules adsorbed on the surface of the biosensor chip. Numerous research group have utilized the SPR technique to investigate biomolecular interactions in real time [8], but only a few articles [9] provide significant information on the temperature dependence of the biomolecular interactions. The main objective of the present work was to determine the binding capacity of kynurenic acid (KYNA) molecules with a model AMPA receptor (AMPAR) peptide fragment by using a novel method published recently [10]. The studied system is of relevance in neuroscience. Glutamate, the main excitatory neurotransmitter in the central nervous system, has been implicated in key processes in the brain, such as synaptic plasticity, memory and learning. However, excessive stimulation of the glutamate receptors (GluRs) may result in neuronal damage, and excitotoxicity has been demonstrated to contribute to

* Corresponding authors at: MTA-SZTE Supramolecular and Nanostructured Materials Research Group, University of Szeged, Hungary. Tel.: +36 62 544210; fax: +36 62 544042.
E-mail addresses: tidecs2000@yahoo.co.uk (E. Csapó), i.dekany@chem.u-szeged.hu (I. Dékány).

http://dx.doi.org/10.1016/j.colsurfb.2015.04.044
0927-7765/

the pathophysiology of acute and chronic neurological disorders, such as stroke, epilepsy or neurodegenerative disorders [11,12]. The main route of tryptophan degradation is through the kynurenine pathway, more than 95% of it being metabolized *via* this metabolic cascade. The kynurenine pathway produces various neuroactive molecules, among them GluR agonists and antagonists. Alterations in the kynurenine pathway have been described in a number of neurological diseases, such as Huntington's disease, migraine and stroke [13,14]. KYNA is of special importance, because it is the only known endogenous antagonist of ionotropic GluRs, and there is increasing evidence suggesting its neuroprotective capacity [15,16]. The neuroprotective effect of KYNA is mainly attributed to the antagonism of the NMDA receptors, but it is also capable of modulating presynaptic glutamate release by antagonizing the α7-nicotinic acetylcholine receptors [17,18]. The possibility of the neuromodulatory role of KYNA in the brain is strengthened by the observation that its action on another type of GluRs, the AMPARs, is concentration-dependent. In micromolar concentrations KYNA is an inhibitor of the AMPARs, while in nanomolar concentrations it has a facilitatory effect on the AMPARs [19,20]. This agonist effect is most probably attributable to allosteric modulation of the extracellular domain, but the exact molecular mechanism is not yet fully understood [19]. Allosteric modulation of the AMPARs has been suggested to be a promising candidate for the treatment of neuropsychiatric disorders such as Parkinson's disease, cognitive impairment or depression [21,22]. An understanding of the exact molecular mechanism of the action of KYNA on the AMPARs might promote future drug development for the therapeutic management of these disorders. In the course of our research work, the human $GluR1_{201–300}$ polypeptide fragment of the AMPARs was studied as this sequence may play a role in the above-mentioned facilitatory effect [19,20]. Three fragments of the polypeptide were synthesized (*ca.* 30 residues/fragment) in order to investigate the affinities of the GluR1 polypeptide fragments toward KYNA drug molecules. The interactions of KYNA with $GluR1_{201–230}$ and $GluR1_{231–259}$ were reported previously [10]. To supplement those results, the $GluR1_{270–300}$ was obtained by solid-phase peptide synthesis and its binding with KYNA was investigated by SPR experiments. Since $GluR1_{270–300}$ does not contain a cysteine residue, the sequence was modified, Trp270 being replaced by Cys270 so as to allow covalent binding to the gold surface *via* the —SH group of Cys270. The presence of the roughly monolayer of the peptide on the gold surface was confirmed by atomic force microscopy (AFM). The cross-sectional area of the peptide was determined by SPR and estimated by theoretical calculations, and molecular modeling techniques were applied to obtain information on possible structure of peptide fragments of $GluR1_{201–300}$ on a pure gold surface. The recently published gold surface model of Iora et al. [23] was utilized in the calculations. After immobilization of the $GluR1_{270–300}$ on the surface of the gold-coated biosensor chip the interaction of KYNA was studied at different temperatures. On the basis of the temperature dependence of the binding of KYNA on the $GluR1_{270–300}$-covered gold surface, the isosteric heat of adsorption (ΔH°/kJ mol^{-1}) was calculated *via* the van't Hoff equation [10]. The isosteric heat of adsorption is defined as the binding enthalpy determined at constant surface coverage [24]. The binding of KYNA to the surface-bonded peptide was also investigated computationally by using the docking procedure implemented in the Glide program [25].

2. Materials and methods

2.1. Materials

KYNA, NaCl, $NaH_2PO_4 \times H_2O$ and $Na_2HPO_4 \times 12\ H_2O$ were purchased from Sigma. $GluR1_{270–300}$ was synthesized in our laboratory and all the amino acids and reagents were purchased from Sigma–Aldrich or Fluka. All the starting materials were used without further purification. The KYNA and peptide stock solutions were freshly prepared, using Milli-Q ultrapure water (18.2 MΩ cm at 25 °C).

2.2. Synthesis of $GluR1_{270–300}$

$GluR1_{270–300}$ (W270C, CKNSDARDHTRVDWKRPKYTSALTY-DGVKVM) was synthesized by a solid-phase technique, utilizing Boc chemistry. The peptide chains were elongated on an MBHA resin (0.76 mmol g^{-1}) and the synthesis was carried out manually. The protecting groups applied were Boc–Asp(OcHex), Boc–Cys(Meb), Boc–Ser(Bzl), Boc–Arg(Tos), Boc–Lys(2ClZ), Boc–Tyr(2BrZ), Boc–His(Z) and Boc–Thr(Bzl). Couplings were performed twice with HBTU. After the final Boc removal, the peptide resin was treated with liquid HF/dimethyl sulfide/*p*-cresol/*p*-thiocresol (86:6:4:2, vol/vol) at 0 °C for 45 min. The HF was then removed and the resulting free peptide was solubilized in 10% aqueous acetic acid, filtered and lyophilized. The crude peptide was purified by semipreparative RP-HPLC on a Phenomenex Jupiter Proteo (Torrance, California) C18 10 μm column (15 × 250 mm). The flow rate was 3 ml min^{-1}, and the gradient was 20–45% in 50 min. The homogeneity of the resulting peptide was evaluated by analytical RP-HPLC on a 4.6 × 250 mm Phenomenex Jupiter 10 C18 300 column at a flow rate of 1.2 ml min^{-1} and a gradient of 24–39% in 15 min. R_t = 9.91. The peptide was further characterized by mass spectrometry with a Waters Acquity quadrupole mass spectrometer equipped with an electrospray ion source. The result: Mw_{calc} = 3640.12, measured for $GluR1_{270–300}$ = 3639.8.

2.3. AFM and SPR spectroscopy

AFM imaging was performed with a PSIA XE-100 (Park Systems) instrument in tapping mode to analyze the peptide-functionalized gold chip and to confirm the presence of a monomolecular peptide layer on the gold surface. The applied cantilever was an antimony-doped single-crystal silicon tip (150 kHz resonant frequency and 5.1 N m^{-1} force constant). SPR measurements were carried out to determine the amount of $GluR1_{270–300}$ peptide adsorbed on the gold chip, and the sorption of KYNA on the peptide-functionalized gold surface. A two-channel SPR sensor platform developed at the Institute of Photonics and Electronics (Prague) was used. The SPR chip is a thin gold layer (50 nm thick) deposited on a glass substrate. During investigations, a flow rate of 25 μl min^{-1} was applied at constant temperature, and the adsorption isotherms were determined at four different temperatures between +10 °C and +40 °C. The interaction of KYNA with the AMPAR subunit was studied in the concentration range 0.1–5.0 mM in phosphate buffer solution at pH 7.40 under physiological conditions (150 mM NaCl). Parallel measurements were performed and the standard deviations of the sorption experiments were ±4.5–5.0%, depending on the temperature. In each step, 500 μl peptide and 500 μl KYNA solutions were injected and the sorption (~20 min) was followed by rinsing with phosphate buffer containing 150 mM NaCl. The SPR spectra were analyzed in real time by a special software package that allows determination of the resonant wavelength in both sensing channels.

2.4. Dynamic light scattering measurements

The dynamic light scattering measurements on $GluR1_{270–300}$ were performed with a Horiba, Nanopartica SZ-100 Nanoparticle Analyzer (He–Ne laser with 532 nm laser wavelength) in order to determine the hydrodynamic diameter (d/nm), electrophoretic mobility (μ/m^2 V^{-1} s^{-1}) and the zeta-potential (ζ/mV). Since the

zeta-potential studies were performed in aqueous solution, the Smoluchowski approximation was used to calculate the zeta-potentials with the aid of the electrophoretic mobility values.

2.5. Theoretical calculations

Our theoretical calculations had the aims of elucidating the structure of the peptide adsorbed on the gold surface and the mode of binding of KYNA to the surface structures. For this, a multistep computer simulation process was carried out. In the first step, a 3D model of the peptide was prepared, using a homology model based on the X-ray structure of the extracellular N-terminal domain of the rat AMPAR (PDB ID: 3saj [26]). The Prime module of the software package of Schrödinger was used to create the model [27]. In the second step, the interaction of the stand-alone peptide with an Au(1 1 1) surface in water was investigated, using the Gromacs molecular dynamics software [28] and the recently published Au surface model of Iora et al. [23]. This method gives a molecular mechanical description of the interactions of the Au(1 1 1) and Au(1 0 0) surfaces with the peptide in water, including surface polarization effects. The peptide was described by a partially modified version of the CHARMM [29,30] forcefield, and the ambient water was modeled by the widely used TIP3P model [31]. Representative structures of the last 10 ns of a 50-ns MD simulation were used to estimate the surface coverage, by simple counting of the covered Au atoms. The next step involved modeling of the surface structures formed by several copies of the peptide in a single layer on the gold surface. For this, we built up a regular 3 by 3 network of the peptide and made a 20-ns, explicit water simulation (using settings similar to those in the stand alone peptide calculations) keeping the center of mass of the eight outer peptides (along the surface) close to the central copy, using a harmonic constraint. This constraint ensures that the average surface coverage remains close to the initial one. Finally, KYNA was docked to randomly selected representative structures obtained from the previous simulation, using the Glide package [25], and the average binding free energy was estimated.

3. Results and discussion

3.1. Immobilization of GluR1$_{270–300}$ on the gold biosensor chip

Since GluR1$_{270–300}$ (sequence presented in Fig. 1) does not contain a Cys residue, the sequence was chemically modified (the Trp at position 270 was replaced by Cys) in order to allow immobilization of the peptide on the gold surface from aqueous solution (c = 0.03 mM) *via* an Au—S covalent bond. The registered SPR sensorgram (Fig. 1a) reveals that 97% of the adsorbed amount remained irreversibly bound on the gold surface after rinsing, and also that no measurable adsorption was detected after *ca.* 80 min indicating that a peptide-covered gold surface was successfully prepared. The binding of the peptide on the gold surface caused a $\Delta\lambda$ = 8.3 nm plasmon shift, which corresponds to an adsorbed amount of GluR1$_{270–300}$ of m^s = 203.0 ng cm^{-2}. The maximal adsorbed amount (m^s/ng cm^{-2}), the adsorption capacity (Γ/nmol cm^{-2}) and the cross-sectional area (a_m/nm^2) of the peptide determined by SPR are presented in Table 1 together with the corresponding data on GluR1$_{201–230}$ and GluR1$_{231–259}$ [10]. Table 1 lists cross-sectional areas ($a_{m,\,calc}$) for the GluR1 peptide fragments and for KYNA calculated by using MarvinSketch [32] and also the average surface coverages obtained from our molecular model. In the current article, the previously published MarvinSketch parameters for each peptide have been refined and both the minimal (A) and maximal (B) projection areas for the lowest-energy conformer are presented. The minimal area of GluR1$_{270–300}$ is 3.28 nm^2, while the maximal area is 5.92 nm^2.[1] The cross-sectional area tentatively determined by SPR (a_m = 2.96 nm^2) is roughly similar to the minimal projection area ($a_{m,\,calc}$ = 3.28 nm^2), indicating that GluR1$_{270–300}$ (supposing a single-layer cover) probably has a compact, well-ordered structure. To study the interaction of this peptide with the gold surface, we carried out a 50-ns simulation for a single GluR1$_{270–300}$ molecule adsorbed on the Au (1 1 1) surface. The interaction of the Cys and Au was observed together with the loss of the original structure of the peptide, which covered 12.2 nm^2 of the gold surface (see Supplementary 1A). This implies that the compact structure (covering only 2.96 nm^2) deduced experimentally is most probably stabilized by the neighboring molecules. Supplementary 1B presents a possible regular arrangement of nine GluR1$_{270–300}$ peptide molecules with a cross-sectional area of ~2.88 nm^2. We additionally built up such regular arrangements for the two peptides studied previously. The corresponding cross-sectional areas for GluR1$_{201–230}$ and GluR1$_{231–259}$ were 2.85 nm^2 and 3.06 nm^2, respectively. We can conclude that the peptide fragments display similar structures on a gold surface. The SPR results and theoretical calculations permit the supposition of the formation of a self-assembled peptide layer on a gold surface [33]. In order to determine the thickness of this peptide layer and to confirm the monolayer coverage of the gold surface, AFM images were recorded. Fig. 1b depicts a representative AFM image of a peptide-covered gold surface (1 × 1 μm area). From an analysis of numerous parts of the peptide film (Fig. 2) it can be concluded that the average thickness of the peptide layer was 2.56 ± 1.05 nm. The line profile, histogram and average thickness data measured at three different sites are to be seen in Fig. 2. Detailed AFM parameters are also presented in Supplementary 2. As peptide aggregation was not observed in the AFM images (Fig. 1b), these results clearly confirm the formation of a roughly monolayer peptide surface on the gold chip under the applied conditions. The theoretical thickness of a self-assembled peptide thin film on a gold surface (~ 3.9 nm; see Supplementary 1B) is in good agreement with the measured AFM data (Fig. 2. and Supplementary 2.) Dynamic light scattering measurement have also been performed to determine the hydrodynamic diameter of the peptide in aqueous solution. According to the results of parallel DLS measurements it was found that the d = 6.75 ± 1.35 nm with PDI = 0.58. The measured diameter is in good agreement with the calculated size (Table 1) of peptide using MarvinSketch [32] software. The zeta-potential value of GluR1$_{270–300}$ were also determined at pH 7.4 in phosphate buffer solution. Since the calculated isoelectric point of this peptide is IEP = 9.74 [32] the measured data is nearly zero (ζ = +0.10 ± 2.2 mV) (μ = 0.000003 cm^2 V^{-1} s^{-1}). Similar IEP values are calculated for GluR1$_{201–230}$ (IEP = 7.30) and GluR1$_{231–259}$ (IEP = 6.32) [32].

3.2. Interaction of GluR1$_{270–300}$ with KYNA on a gold surface

In order to determine the binding capacity and also the isosteric heat of adsorption of KYNA on the peptide-covered gold surface, the binding of KYNA on a GluR1$_{270–300}$-functionalized biosensor chip was investigated at four different temperatures in the concentration range 0.1–5.0 mM. Sensorgrams registered at +10 °C and +30 °C are presented in Fig. 3. These indicate that an increase in the concentration of the KYNA solution from 0.1 mM to 5.0 mM results in a shift to higher wavelength of from ~ 0.2 nm to almost 1 nm at both temperatures (similar changes were seen at +20 °C and +40 °C too). The sensorgrams confirm that the interaction between KYNA and GluR1$_{270–300}$ is fully reversible because the adsorbed mass of KYNA fell to nearly zero on rinsing. The maximal plasmon shifts caused by KYNA binding on GluR1$_{201–230}$ ($\Delta\lambda$ = 1.85) and GluR1$_{231–259}$

[1] The minimal and maximal projection areas were determined for free molecules (not on the gold surface).

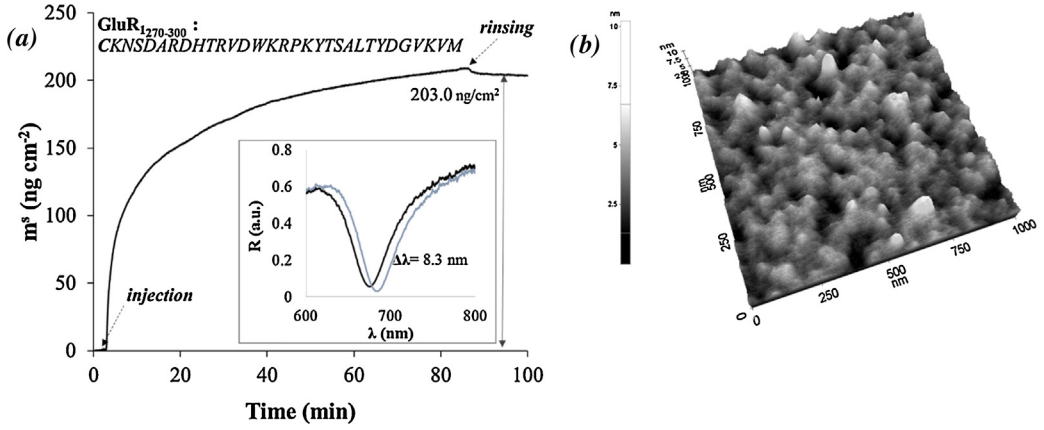

Fig. 1. Binding of GluR1$_{270–300}$ on a bare gold surface (c = 0.03 mM, I = 150 mM) (KCl), pH = 7.40, T = 20 °C, flow rate: 25 μl min^{-1}, experimental error ±4.5%; the inset shows plasmon resonance curves before and after binding (a) and a representative AFM image of the monolayer peptide-functionalized gold surface (b).

Table 1
Maximal adsorbed amount (m^s), adsorption capacity (Γ), and measured (a_m) and calculated ($a_{m,\,calc}$) cross-sectional areas for KYNA, GluR1$_{201–230}$, GluR1$_{231–259}$ and GluR1$_{270–300}$. The calculated areas were estimated for free molecules (3D) and for molecules on the gold surface (2D).

Molecules on gold surface at 20 °C	m^s (ng cm^{-2})	Γ (nmol cm^{-2})	a_m (nm^2)	$a_{m,\,calc}$ (nm^2) free molecules[a]		$a_{m,\,calc}$ (nm^2) peptide on Au(1 1 1) surface	
				(A)	(B)	(A)	(B)
KYNA	130.0[b]	0.687[b,c]	0.242[b]	0.28	0.63	–	–
GluR1$_{201–230}$	198.8[b]	0.059[b]	2.814[b]	3.76	4.99	2.85	11.80
GluR1$_{231–259}$	204.5[b]	0.064[b]	2.594[b]	3.25	7.04	3.06	13.00
GluR1$_{270–300}$	203.0	0.056	2.964	3.28	5.92	2.88	12.20

$\Gamma = m^s/M_w$; $a_m = 0.166 \times (1/\Gamma)$.
[a] The $a_{m,\,calc}$ values for the free peptides and KYNA were calculated by using MarvinSketch [32].
[b] Previously published data [10].
[c] The monolayer adsorption capacity determined from the KYNA adsorption isotherm (T = 20 °C).

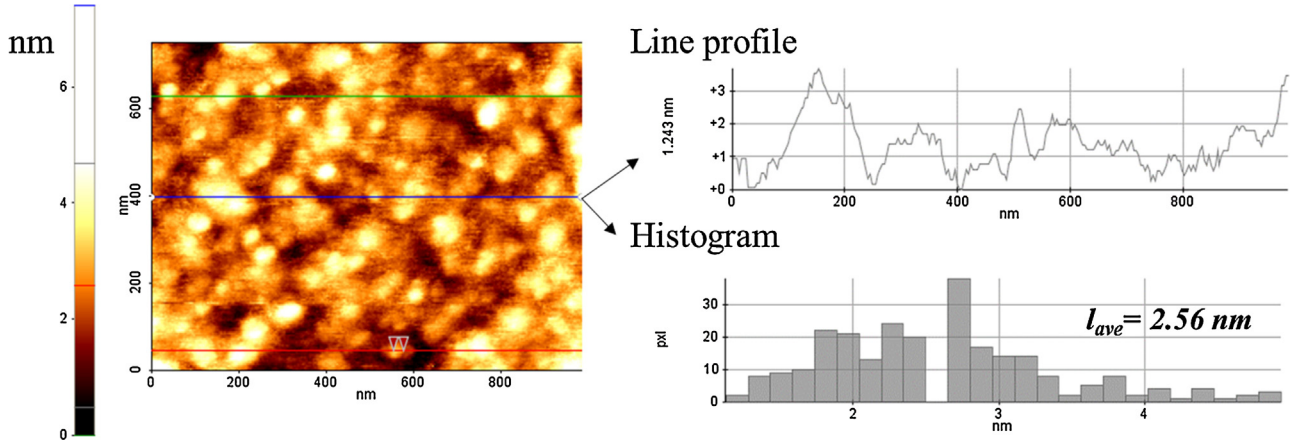

Fig. 2. Cross-sectional analysis of a GluR1$_{270–300}$-functionalized gold SPR chip *via* the AFM technique.

Table 2
Adsorbed monolayer amount (m^s) and monolayer adsorption capacity (Γ_m) of KYNA on different peptide-modified gold surfaces and binding enthalpy (ΔH°) values at the minimum of the ΔH° vs. Θ function.

KYNA on peptide-functionalized gold surface		m^s (ng cm^{-2})	Γ_m (nmol cm^{-2})[a]	ΔH°_{min} (kJ mol^{-1})	$n_{peptide}$:n_{KYNA} at ΔH°_{min}	Ref.
GluR1$_{201–230}$	(10 °C)	18.9	0.100			
	(20 °C)	16.8	0.089	−39.21 ± 0.25	1:1.3	[10]
	(30 °C)	15.1	0.080			
	(40 °C)	14.4	0.076			
GluR1$_{231–259}$	(10 °C)	19.9	0.105			
	(25 °C)	18.2	0.096	−37.99 ± 0.42	1:1.4	[10]
	(40 °C)	17.6	0.093			
GluR1$_{270–300}$	(10 °C)	15.9	0.084			
	(20 °C)	13.8	0.073	−29.64 ± 0.25	1:1.07	
	(30 °C)	11.7	0.062			
	(40 °C)	10.4	0.055			

[a] Calculated by using the BET equation ([10], Eq. 3).
$m^s = \Gamma_m \times M_{w,\,KYNA}$.

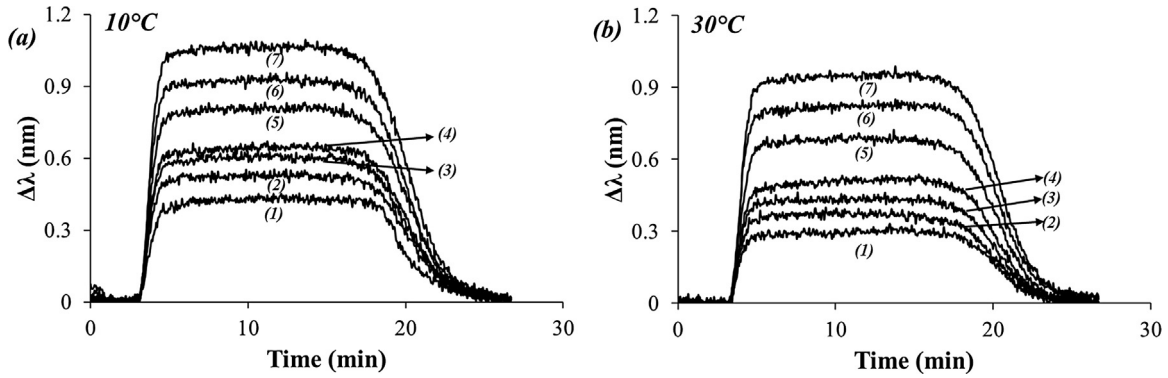

Fig. 3. Representative SPR curves of binding of KYNA to the GluR1$_{270–300}$-functionalized gold surface at different temperatures (I = 150 mM (KCl), pH = 7.40, flow rate: 25 μl min^{-1}). The experimental error is ±4.5% at 10 °C and ±4.8% at 30 °C. The concentrations of KYNA solutions: 0.5 (*1*); 1.0 (*2*); 1.5 (*3*); 2.0 (*4*); 3.0 (*5*); 4.0 (*6*); 5.0 (*7*) mM for (a), and 0.1 (*1*); 0.5 (*2*); 1.0 (*3*); 1.5 (*4*); 3.0 (*5*); 4.0 (*6*); 5.0 (*7*) mM for (b).

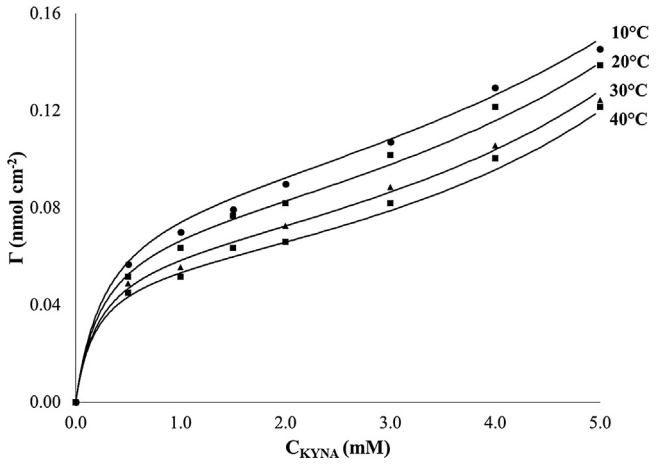

Fig. 4. Adsorption isotherms at different temperatures of KYNA on the gold SPR chip surface after functionalization with GluR1$_{270–300}$ (experimental error ±4.8%); the R^2 = 0.9943 (10 °C), R^2 = 0.9948 (20 °C), R^2 = 0.9959 (30 °C), R^2 = 0.9900 (40 °C).

(Δλ = 1.84) [10] were higher than that on GluR1$_{270–300}$ (Δλ = 1.10) covered gold biosensor chips at +10 °C, reflecting the less reversible binding of KYNA on the latter surface. Adsorption isotherms of the GluR1$_{270–300}$–KYNA system derived from SPR experiments at various temperatures are depicted in Fig. 4. Similarly as for the GluR1$_{201–230}$–KYNA and GluR1$_{231–259}$–KYNA systems [10], the adsorption isotherms for the GluR1$_{270–300}$–KYNA interaction were fitted with the Brunauer–Emmet–Teller (BET), Langmuir and Freundlich isotherm equations [34,35]. The R^2 values calculated by least-squares curve fitting (R^2 > 0.99) (BET), R^2 > 0.95 (Langmuir) and R^2 > 0.98 (Freundlich) indicated that the BET isotherm function (Eq. 3 in Ref. [10]) closely follows the trend in the measured data (suggesting a multilayer adsorption model). In consequence of the reversible adsorption of KYNA on the GluR1$_{270–300}$ surface, the isosteric heat of adsorption could be determined *via* the isotherms. The monolayer binding capacity data (Γ_m) for KYNA on the peptide-functionalized gold surface (Table 2), obtained through the BET equation [10], demonstrated that more KYNA was reversibly bound on the GluR1$_{201–230}$ (0.100 and 0.076 nmol cm^{-2}) and GluR1$_{231–259}$ (0.105 and 0.093 nmol cm^{-2}) covered surfaces at 10 °C and 40 °C than in the case of GluR1$_{270–300}$ (0.084 and 0.055 nmol cm^{-2}) (Fig. 5a). Binding enthalpy (isosteric heat of adsorption) evaluated as previously are presented [10] as a function of the surface loading of KYNA ($\Theta = \Gamma_{KYNA}/\Gamma_{m,KYNA}$) in Fig. 5b. The trends observed for the studied systems are apparently similar, an increase in the surface coverage to $\Theta \sim 1$ resulting in a steady increase in the isosteric heat of adsorption. When Θ is further increases to ~2.5, the ΔH° continually decreases. On the other hand, a detailed comparison of the ΔH° vs. Θ functions reveals measurable differences between the enthalpy values of the studied systems at the minimum of the ΔH° vs. Θ function (ΔH°_{min}). The isosteric heats of adsorption for KYNA on GluR1$_{201–230}$ (-39.21 ± 0.25 kJ mol^{-1}) and GluR1$_{231–259}$ (-37.99 ± 0.42 kJ mol^{-1}) were higher than that on the GluR1$_{270–300}$ (-29.64 ± 0.25 kJ mol^{-1})-functionalized gold thin films. It seems likely that at low KYNA concentrations ($\Theta \sim 0.1–0.3$) the binding sites of the peptide are unavailable to KYNA but that at $\Theta \sim 1$ the structure of the peptide may change (possibly partially unfolding due to the increase in KYNA concentration), resulting in free binding sites for the KYNA molecules. At high surface coverage (Θ > 1.5)

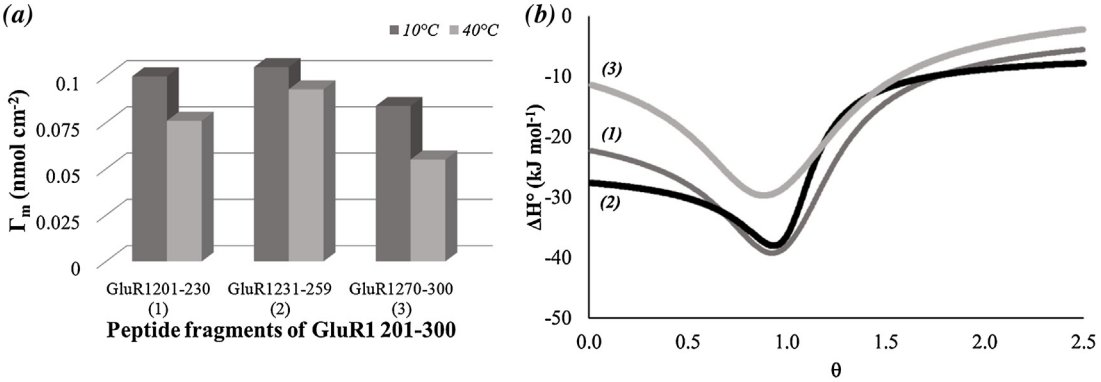

Fig. 5. Amounts of KYNA bonded at 10 °C and 40 °C (a) and binding enthalpies of KYNA on a GluR1$_{201–230}$ (1), GluR1$_{231–259}$ (2) and GluR1$_{270–300}$ (3)-functionalized gold thin film as a function of surface coverage (b). Standard error: 1%.

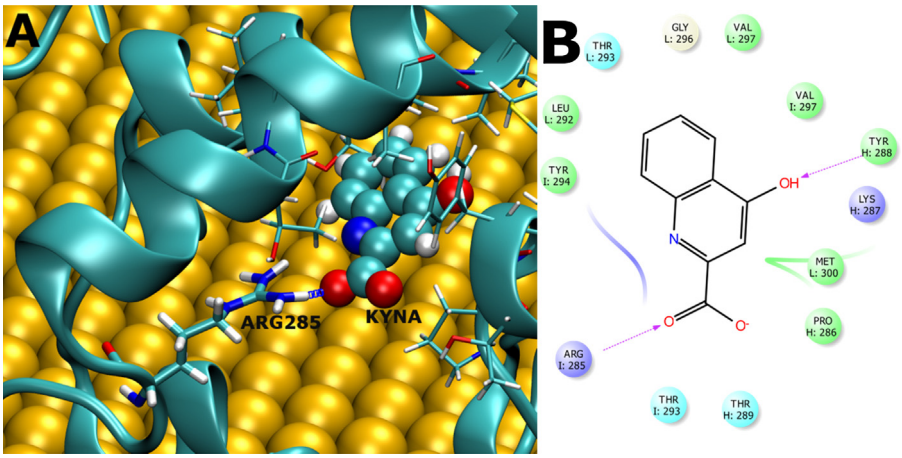

Fig. 6. (A) A representative binding mode of KYNA docked to GluR1$_{270–300}$ bonded on the Au(1 1 1) surface, and (B) its interaction map.

measurably less interactions between KYNA and the peptides are observed (the KYNA–KYNA interactions may be more pronounced). At the minimum of the ΔH° vs. Θ function, the peptide:KYNA molar ratios were calculated (Table 2) for all three peptide–KYNA systems. For the GluR1$_{201–230}$–KYNA and GluR1$_{231–259}$–KYNA interactions, the highest enthalpy was measured at an $n_{peptide}$:n_{KYNA} ratio of ~1:1.5, whereas for GluR1$_{270–300}$–KYNA the corresponding ratio was nearly 1:1.

3.3. Theoretical calculations

Randomly selected structures obtained from the 20-ns, explicit water molecular dynamics simulation setting out from the regular peptide structures on the Au(1 1 1) surface were used as targets for molecular docking calculations. The Glide program was parameterized to find binding sites in the inner and the water-exposed upper regions of the peptides. In the large majority of the binding positions found, KYNA binds to a positively charged residue (Arg or Lys), forming a salt bridge, with the benzene ring situated in a nearby apolar pocket. Fig. 6 presents a possible binding position of KYNA connected to the surface structures of GluR1$_{270–300}$, together with the interaction map. The binding free energy (ΔG) can be estimated from the averaged highest Glide score values calculated for the best binding positions. We obtained −29, −25 and −31 kJ mol^{-1} for GluR1$_{201–230}$, GluR1$_{231–259}$ and GluR1$_{270–300}$, respectively, i.e. GluR1$_{231–259}$ binds somewhat more weakly than the other two. These estimated binding free energy values are in good agreement with the tentatively determined order of magnitude of the binding enthalpies, suggesting weak second-order interactions between the peptides and KYNA. It must be borne in mind that, in our theoretical model, only a few peptide molecules are bound on the gold surface and a single KYNA is docked onto these peptides, while in our SPR experiments the KYNA sorption was measured on an extended monolayer peptide surface. The lateral interaction between the neighboring surface-bonded peptide molecules could influence their surface arrangement and thereby modify the KYNA binding.

4. Conclusion

GluR1$_{270–300}$ was immobilized on a gold thin film *via* covalent (Au—S) bonding resulting in the formation of a self-assembled monolayer peptide surface on a gold biosensor chip, as confirmed by AFM. The binding of kynurenic acid to the peptide-functionalized gold surface proved to be fully reversible. The amounts of KYNA adsorbed on GluR1$_{201–230}$ and GluR1$_{231–259}$ modified gold surfaces at different temperatures under physiological conditions were higher than that on the GluR1$_{270–300}$-functionalized surface. Both the experimental results and molecular docking calculations support the occurrence of weak second-order interactions between KYNA and peptide fragments of GluR1$_{201–300}$. The two-dimensional sensor technique applied has been used to provide important information for the design of core-shell type nanoparticles containing protein-based drug molecules for controlled drug delivery. These core-shell nanoparticles are widely used in diagnosis and therapy to deliver a drug to the right place at the right time in adequate concentration. Identification and quantification of the physical–chemical properties of the nanocarrier composite systems are crucial for developing. The SPR results supply information (e.g. aspects of the protein–drug molecule interactions; binding capacity of proteins; adsorption–desorption kinetics; etc.) on the interactions between proteins and drug molecules (e.g. KYNA).

Acknowledgements

This research was supported by the European Union and the State of Hungary, co-financed by the European Social Fund in the framework of TÁMOP-4.2.2.A-11/1/KONV-2012-0047, by the Hungarian Brain Research Program (NAP. Grant No. KTIA-13-NAP-AIII/9) and by EUROHEADPAIN (FP7-Health 2013-Innovation; Grant No. 602633). The authors thank Judit Kopniczky and Viktória Hornok (University of Szeged) for the AFM measurements.

Appendix A. Supplementary data

Supplementary data associated with this article can be found, in the online version, at http://dx.doi.org/10.1016/j.colsurfb.2015.04.044

References

[1] J. Vörös, J.J. Ramsden, G. Csúcs, I. Szendrő, S.M. De Paul, M. Textor, N.D. Spencer, Biomaterials 23 (2002) 3699.
[2] H. Sípová, J. Homola, Anal. Chim. Acta 773 (2013) 9.
[3] J.F. Masson, T.m. Battaglia, S. Beaudoin, K.l. Booksh, Smart medical and biomedical sensor technology II, in: B.M. Cullum (Ed.), Proceedings of SPIE, vol. 5588, SPIE, Bellingham, WA, 2004.
[4] J. Vörös, Biophys. J. 87 (2004) 553.
[5] W.A. Murray, W.L. Barnes, Adv. Mater. 19 (2007) 3771.
[6] L.S. Jung, C.T. Campbell, T.M. Chinowsky, M.N. Mar, S.S. Yee, Langmuir 14 (1998) 5636.
[7] D. Sebők, E. Csapó, T. Preocanin, G. Bohus, N. Kallay, I. Dékány, Croat. Chem. Acta 86 (2013) 287.

[8] M. Vala, R. Robelek, M. Bocková, J. Wegener, J. Homola, Biosens Bioelectron. 40 (2013) 417.
[9] N. Singh, S.M. Husson, Biomacromolecules 6 (2005) 9.
[10] E. Csapó, Z. Majláth, Á. Juhász, B. Roósz, A. Hetényi, G.K. Tóth, J. Tajti, L. Vécsei, I. Dékány, Colloids Surf. B 123 (2014) 924.
[11] D. Zádori, P. Klivényi, L. Szalárdy, F. Fülöp, J. Toldi, L. Vécsei, J. Neurol. Sci. 322 (2012) 187.
[12] I. Obál, Z. Majláth, J. Toldi, L. Vécsei, J. Parkinson's Dis. 4 (2014) 139.
[13] L.G. Darlington, G.M. Mackay, C.M. Forrest, N. Stoy, C. George, T.W. Stone, Eur. J. Neurosci. 26 (2007) 2211.
[14] L. Vécsei, L. Szalárdy, F. Fülöp, J. Toldi, Nat. Rev. Drug. Discov. 12 (2013) 64.
[15] D. Zádori, P. Klivényi, E. Vámos, F. Fülöp, J. Toldi, L. Vécsei, J. Neural. Transm. 116 (2009) 1403.
[16] Z. Majlath, J. Toldi, L. Vécsei, J. Neural. Transm. 121 (2014) 881.
[17] R. Carpenedo, A. Pittaluga, A. Cozzi, S. Attucci, A. Galli, M. Raiteri, F. Moroni, Eur. J. Neurosci. 13 (2001) 2141.
[18] C. Hilmas, E.F. Pereira, M. Alkondon, A. Rassoulpour, R. Schwarcz, E.X. Albuquerque, J. Neurosci. 21 (2001) 7463.
[19] C. Prescott, A.M. Weeks, K.J. Staley, K.M. Partin, Neurosci. Lett. 402 (2006) 108.
[20] E. Rózsa, H. Robotka, L. Vécsei, J. Toldi, J. Neural. Transm. 115 (2008) 1087.
[21] S.E. Ward, M. Harries, Curr. Med. Chem. 30 (2010) 3503.
[22] M.J. O'Neill, D. Bleakman, D.M. Zimmerman, E.S. Nisenbaum, Curr. Drug Targets CNS Neurol. Disord. 3 (2004) 181.
[23] F. Iori, R. Di Felice, E. Molinari, S. Corni, J. Comput. Chem. 30 (2009) 1465.
[24] P. Saha, S. Chowdhury, Insight into adsorption thermodynamics, in: M. Tadashi (Ed.), Thermodynamics, InTech, 2011, ISBN 978-953-307-544-0, http://www.intechopen.com/books/thermodynamics/insight-into-adsorption-thermodynamics
[25] Glide, v6.5, Schrödinger, LLC, New York, NY, 2014.
[26] G.R. Yao, Y.N. Zong, S.Y. Gu, J. Zhou, H.X. Xu, I.I. Mathews, R.S. Jin, Biochem. J. 438 (2011) 255.
[27] Prime, v3.8, Schrödinger, LLC, New York, NY, 2014.
[28] B. Hess, C. Kutzner, D. van der Spoel, E. Lindahl, J. Chem. Theory Comput. 4 (2008) 435.
[29] A.D. MacKerell, D. Bashford, M. Bellott, R.L. Dunbrack, J.D. Evanseck, M.J. Field, S. Fischer, J. Gao, H. Guo, S. Ha, D. Joseph-McCarthy, L. Kuchnir, K. Kuczera, F.T.K. Lau, C. Mattos, S. Michnick, T. Ngo, D.T. Nguyen, B. Prodhom, W.E. Reiher, B. Roux, M. Schlenkrich, J.C. Smith, R. Stote, J. Straub, M. Watanabe, J. Wiorkiewicz-Kuczera, D. Yin, M. Karplus, J. Phys. Chem. B 102 (1998) 3586.
[30] A.D. Mackerell, M. Feig, C.L. Brooks, J. Comput. Chem. 25 (2004) 1400.
[31] W.L. Jorgensen, J. Chandrasekhar, J.D. Madura, R.W. Impey, M.L. Klein, J. Chem. Phys. 79 (1983) 926.
[32] MarvinSketch, http://www.chemaxon.com/products/marvin/marvinsketch
[33] M.A. Wolak, A. Balaeff, S. Gutmann, H.J. Helmrich, R. Vosloo, et al., J. Phys. Chem. C 115 (2011) 17123.
[34] X. Li, S.M. Husson, Biosens Bioelectron. 22 (2006) 336.
[35] S. Yamaguchi, T. Mannen, T. Zako, N. Kamiya, T. Nagamune, Biotechnol. Prog. 19 (2003) 1348.